JOURNAL OF SPACECRAFT AND ROCKETS
Vol. 48, No. 3, May–June 2011

Rigidizable Inflatable Get-Away-Special Experiment Space Flight Data Analysis

Jonathan T. Black,* Richard G. Cobb,* Eric D. Swenson,* and Brett J. Cooper†
Air Force Institute of Technology, Wright–Patterson Air Force Base, Ohio 45433

DOI: 10.2514/1.50939

The rigidizable inflatable get-away-special experiment was run successfully onboard STS-123 (Endeavour) in March 2008. The experiment was designed and built by graduate students at the Air Force Institute of Technology, and returned there following the shuttle flight for postflight analysis. The experiment's objectives were to demonstrate in space the stowage, deployment, and rigidization techniques of carbon fiber composite inflatable rigidizable cylindrical booms. It was a canister-for-all-payload-ejections space shuttle cargo bay experiment, during which three 50.8 cm- (20 in.)-long carbon fiber composite booms were heated and inflated in a microgravity vacuum environment, and the structural characteristics and the deployment accuracy of the booms were examined. All three booms deployed and rigidized, completing all primary mission objectives. Pressure, temperature, modal response, and position data were collected successfully on orbit and compared here with ground test data. This research demonstrates the feasibility of using lightweight and low stowage volume (high packaging ratio) inflatable/rigidizable space structures for space mission applications.

I. Introduction

INFLATABLE space structures have long been acknowledged as a means of reducing complexity, weight, volume, and cost of large space systems. Beginning with the limited launch capabilities of the early space program, inflatable structures were used successfully in orbit multiple times [1]. Lack of understanding of the deployment processes in space coupled with large increases in lift capacity led the early space community to use more familiar metal structures. Spacecraft complexity has increased with increasing demands levied on the system's performance, which drives increases in spacecraft weight and stowed volume for launch. It can be shown that increasing weight and volume increases overall spacecraft and launch costs, while limiting the potential number of space lift providers [2].

As in the early space program, inflatable structures are again being investigated to reduce spacecraft weight, volume, and cost. However, inflatable space structures still present many challenges, such as maintaining internal pressure for structural integrity. Though recent inflatable space experiments have gone several years without mission ending pressure loss events, it is conceivable that pressure loss would weaken the entire structure, possibly ending the mission [3]. For a pure inflatable structure, there are few means to combat this limitation. An alternative to continual pressurization is to rigidize the structure after inflation.

Over the last two decades the majority of the work associated with inflatable/rigidizable space structures has been confined to computer modeling and ground testing of deployment and structural characteristics. The Jet Propulsion Laboratory and NASA Langley Research Center conducted a series of tests from approximately 1999 to 2003 to develop a database of the structural characteristics of inflatable rigidizable booms. Several dozen cylindrical hollow tubes (booms) with length over diameter ratios of 10 or higher were tested statically and dynamically. Tube diameters were all between 10.16 and 15.24 cm (4 and 6 in.). Dynamic testing was conducted under fixed-free boundary conditions using impact hammers and miniature accelerometers to determine the effective elastic and shear moduli of the booms. The rigidized tubes proved sufficiently stiff as to be amenable to this type of impact testing [4–6].

To demonstrate that excitation could be actively controlled using embedded piezoactuators, several macrofiber composite (MFC) actuators were embedded in composite inflatable rigidizable tubes identical to those described. A laser vibrometer was used to measure the free decay vibration of the tubes from impacts. It was found that active MFC actuators could increase the damping of the first bending mode from 0.4 to 8% [4,7,8].

Large aperture space-based mirrors are one application of lightweight inflatable technology, and thus several membrane-based, torus-supported apertures, including solar thermal concentrators and antenna, were dynamically tested at NASA Marshall Space Flight Center. Most of these were tested in fixed-free boundary conditions in which the metal end caps of the composite rigidizable support struts were mechanically secured to the ground. Shakers were attached to the metal end caps to provide excitation. A laser vibrometer was selected as the measurement device in these tests because of the noncontact nature of the measurements [1,4,9–12].

The tests described in [13–20] used adaptations of traditional dynamic testing methods to characterize pressurized tori. In [13,14] a 1.8 m diameter pressurized Kapton torus was tested at different internal pressures using an impact hammer. The hammer was modified by attaching a small aluminum plate to the hammer head instead of a traditional tip to spread the applied impulse out over a wider area, and a small accelerometer measured its response. Excitation using a traditional tip would have caused local buckling. The first three in- and out-of-plane mode shapes were observed at pressures above 0.8 psig, but despite the modifications to the hammer, it was still unable to globally distribute the excitation energy, leading to poor coherence and unsatisfactory dynamic identification results.

A similar 1.8 m diameter torus composed of a 0.15 m diameter Kapton tube pressurized to 0.5 psi was tested in [15–19]. In these tests, the piezoactuator MFC patches were used as both the actuators and sensors. Multiple MFC patches were attached to the surface of the torus at various intervals from each other, and structural natural frequencies, out-of-plane mode shapes, and damping values were obtained from the data. These tests were also performed with a membrane mirror attached to the torus to determine the boundary interactions of the two structures. Finally, in addition to excitation and measurement, the MFC actuators were used to control the structure, obtaining up to a 70% reduction in the amplitude of vibrations.

Presented as Paper 2009-2157 at the 50th AIAA/ASME/ASCE/AHS/ASC Structures, Structural Dynamics, and Materials Conference, Palm Springs, CA, 4–7 May 2009; received 24 June 2010; revision received 28 September 2010; accepted for publication 28 September 2010.

*Assistant Professor, Department of Aeronautics and Astronautics, 2950 Hobson Way. Associate Fellow AIAA.

†Student, Department of Aeronautics and Astronautics, 2950 Hobson Way. Student Member AIAA.

The primary objective of the Rigidizable Inflatable Get-Away-Special Experiment (RIGEX) was to demonstrate and validate deployment and rigidization techniques for three 50.8 cm (20 in.) long carbon fiber booms (tubes) in a microgravity environment. Inflation, deployment, and rigidization methodology, hardware design, and initial preflight ground results are presented in [21]. Temperature and pressure flight data are presented here, along with the tubes' rigidized structural and physical characteristics measured on orbit using adaptations of the described techniques for correlation with ground test data. The recent space test was a successful proof of concept demonstration, and will result in a technology readiness level (TRL) increase for the future use of inflatable/rigidizable technology to help alleviate payload mass and volume limitations.

II. Experiment Description

RIGEX was an experiment mounted inside the canister for all payload ejections (CAPE) attached to the rear of the space shuttle cargo bay (Fig. 1) [22]. The experiment used shuttle power for testing purposes while being exposed to the ambient space vacuum, temperature, and microgravity. The experiment was cylindrical as specified by the NASA CAPE payload envelope. The experiment maximized the CAPE weight and volume constraints at 159 kg, and 53 cm in diameter and 135 cm in height.

The RIGEX experiment consisted of three tube bays and a computer bay, arranged radially about an open center which stored the pressure tanks for inflation. Figure 2 shows a computer-aided drawing (CAD) representation of RIGEX. Immediately visible are two inflatable/rigidizable experiment bays; the right bay shows an inflated and rigidized boom rising out of an unlatched oven box, and the left bay shows a stowed boom. The tubing required for boom inflation can be seen at the bottom of Fig. 2. Above the booms are cameras, and attached to the tip of the booms are accelerometers.

The inflatable, rigidizable tubes consist of a three ply carbon fiber layup and a proprietary thermoplastic resin based on a polyurethane elastomer. The material is designed to transition from rigid to pliable at a glass-transition temperature (T_g) of 125°C. RIGEX used resistive heaters to heat the prefolded tubes above the glass-transition temperature, at which point the ovens turned off and unlatched, allowing the tubes to freely deploy. Residual strain energy stored during the stowing process deployed the tube slightly upon release of the oven latches, at which point nitrogen gas was injected into the tubes, bringing them to a fully deployed configuration. After inflation, the tubes cooled below the transition temperature, rigidized, and vented the nitrogen. The tubes were then excited by two MFC piezoelectric patches mounted near the fixed end. The MFC patches were designed by NASA Langley for vibration response testing.

Aside from external power from the shuttle, RIGEX was a wholly self-contained experiment. Power was required for the computer, ovens, cameras, light emitting diodes (LEDs), MFC patches, and accelerometers. The shuttle provided RIGEX with direct current power for the resistive heaters. While in space, the only interface with RIGEX was an on–off toggle switch and display indicator on the Standard Switch Panel accessible to the astronauts in the middeck. The experiment therefore ran autonomously from start to finish over the course of several hours. More details of the experiment design, configuration, and performance can be found in [21].

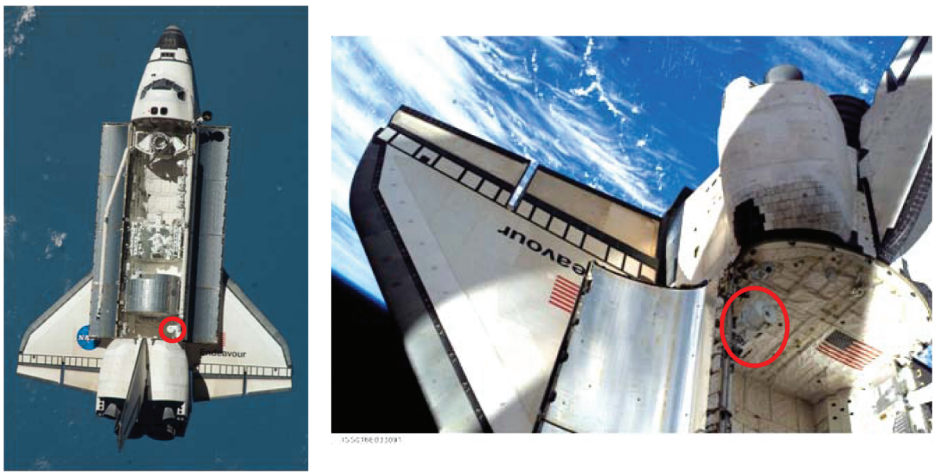

Fig. 1 RIGEX in Endeavour (STS-123) cargo bay highlighted by circle (courtesy of NASA).

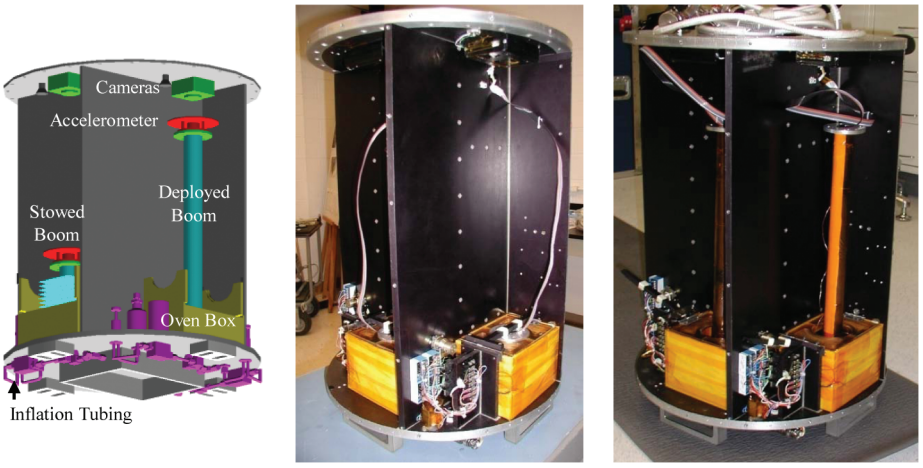

Fig. 2 RIGEX CAD representation showing experiment bays (left), before shuttle integration (center) and following shuttle return (right).

III. Data Collection

The RIGEX data collection activities are divided into those tests that occurred while the shuttle was on orbit and those tests that occurred postflight at the Air Force Institute of Technology (AFIT). The deployment phase collections occurred on orbit during the physical processes necessary to deploy the booms from their stowed configurations. The postdeployment data collections occurred during the vibration response testing conducted immediately after the deployment. The postflight data collections occurred after the experiment was removed from Endeavour and returned to AFIT.

RIGEX was activated during quiescent operations on Flight Day 14 (24 March 2008) of STS-123. Pressure and temperature data were collected during boom deployment, and acceleration data was collected postboom deployment. Postflight data consists of laser-based three dimensional (three-dimensional) physical alignment measurements of the deployed tubes and further vibration testing of the deployed tubes using higher fidelity ground test hardware such as laser Doppler velocimeters.

A. Deployment

The deployment phase began with an astronaut toggling the RIGEX power switch on the standard switch panel to "on," which supplied power to the experiment. Upon receiving power, the computer automatically booted up and ran through a variety of memory verifications. Temperature data was collected from thermocouples attached to the computer board and base of the experiment structure. After recording the pressure of the nitrogen storage tanks, the computer turned on the resistive heater oven in bay 1, which began radiating heat and warming tube 1. LEDs illuminated the bay, and the camera at the top of the bay collected an image every 50 s. Two K-type thermocouples mounted inside the tube folds recorded the tube temperature, and after the tubes warmed sufficiently above the glass-transition temperature of 125°C, the accelerometers at free ends of the tubes activated and the oven door latch released, allowing the doors to open. After the oven doors opened, pressure transducers began to monitor pressure inside of the valve connecting the boom to the nitrogen storage tank which then opened, and nitrogen gas filled the tube. The pressure equalized after the tube completely inflated (in less than 5 s), and pressure and acceleration recordings ended 5 s after they began. The camera then stopped taking pictures, the LEDs turned off, and temperature recording ceased. After a 5 min hold to cool and rigidize the boom, the inflation valve was moved to the vent position, venting the nitrogen inflation gas to ambient, and concluding the deployment phase for tube 1. The exact same process was followed for the next two tubes, as depicted in Fig. 3. Figure 4 shows a stowed tube z-folded for launch and a deployed tube, respectively.

B. Postdeployment

The postdeployment phase began after each tube had cooled and rigidized. This phase involved five minutes of forced vibration response testing, using the 5-cm-long MFC patches attached to the base of the tubes and triaxial accelerometers attached to the free end cap. After each tube cooled for five minutes, a 0–2000 Hz chirp signal was applied to the MFC patches over a period of 1 s.

The computer sample rate was 5000 Hz. During each excitation event, the tube tip triaxial accelerometers monitored and recorded acceleration data. After 25 1 s excitations of each tube, the post-deployment phase was complete for that particular tube and the experiment moved to deployment phase for the next tube. After

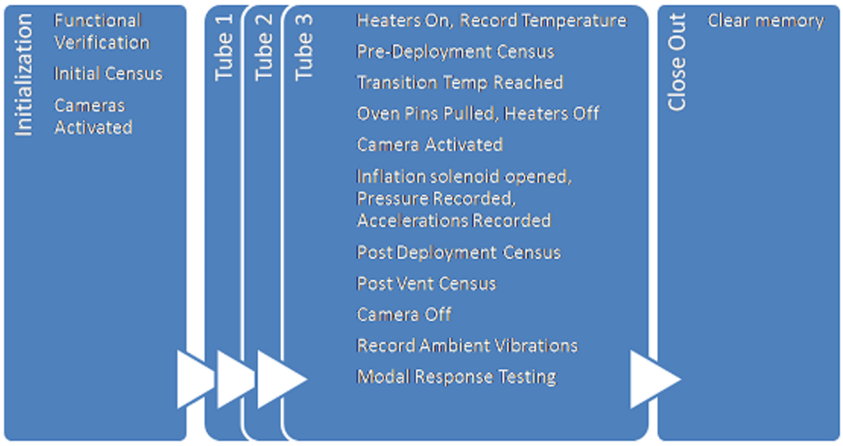

Fig. 3 RIGEX experiment timeline.

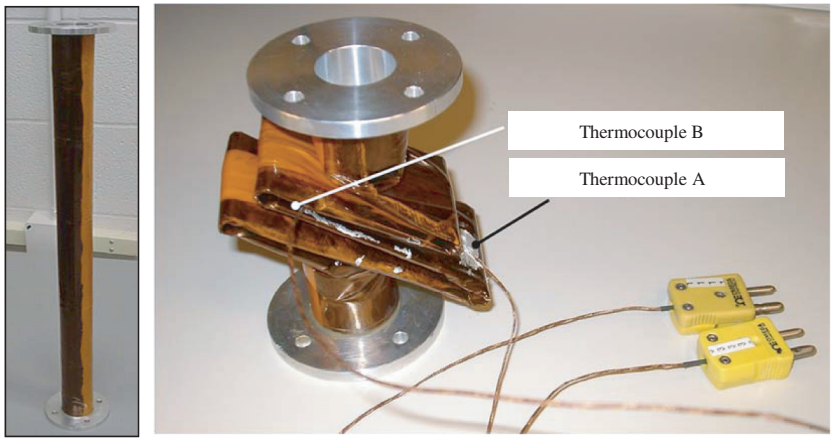

Fig. 4 Deployed and stowed RIGEX booms. Thermocouple locations on stowed tube.

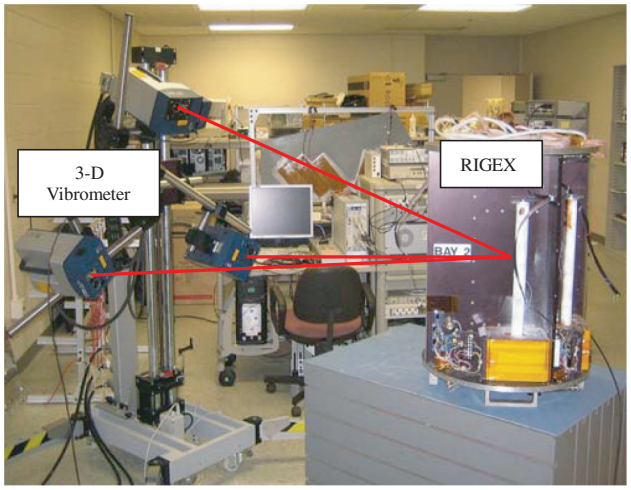

Fig. 5 Postflight three-dimensional scanning laser vibrometer test setup.

postdeployment phase activities were complete for tube 3, the computer set the display on the standard switch panel to indicate experiment completion and the astronauts later toggled the power switch to "off."

C. Postflight

Postflight data collection activities are defined to be the vibration and position change detection tests that occurred after the experiment had been off-loaded from Endeavour following the flight and returned to AFIT. All experimental data was copied at Kennedy Space Center and the experiment was packed and shipped to AFIT. When RIGEX arrived at AFIT, it was unpacked and examined for any changes that may have occurred during shipment.

The first postflight data collection was a precision three dimensional physical alignment measurement, conducted with a seven-axis 2 m robotic arm with a hard probe accurate to 0.01 mm. The measurements produce three-dimensional point clouds which were then imported into three-dimensional CAD models. The measured points are compared with perfectly straight tube deployments and distance measurements are taken to determine deployment errors.

The next test was used to determine ground truth vibration response data for comparison to flight data, as well as previous lab-based vibration data from similar tubes. A three-dimensional scanning laser vibrometer was used to measure the forced vibration response in user-defined orthogonal x-, y-, and z-directions. The signal analyzer/user interface software was used to align the laser heads and generate a grid of scan points. By combining the measured velocity from all three vibrometer heads, the system generates three-dimensional frequency response functions (FRFs) and calculates the operating deflection shapes corresponding to peaks in the FRFs. The flight MFC piezoelectric patches excited the tubes with externally-generated 0–500 and 0–5000 Hz chirp signals to ensure sufficient resolution to capture low frequency modes and a wide enough bandwidth to fully-characterize the tubes. Figure 5 shows the postflight lab test setup.

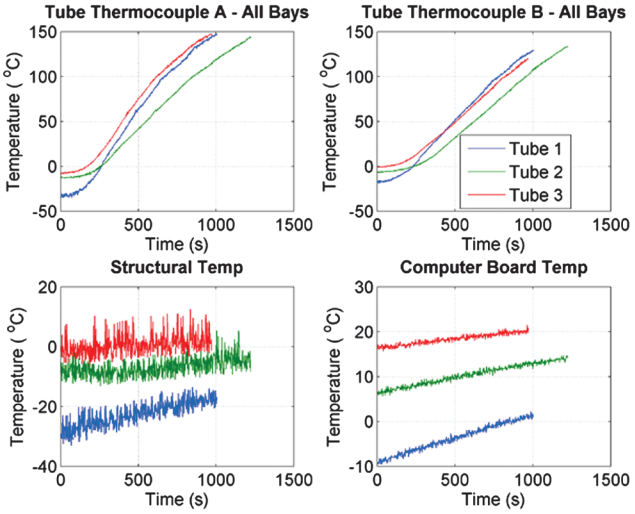

Fig. 6 Deployment temperature versus time for all thermocouple locations.

IV. RIGEX Test Results and Analysis

Data analysis began immediately after RIGEX was removed from Endeavour upon its return to Earth. All of the flight data was copied from the onboard computer and several pictures of the experiment and deployed tubes were taken, showing that the experiment deployed all three tubes thereby successfully completing its primary objectives (Fig. 2). RIGEX was then shipped to AFIT for data analysis and postflight testing.

A. Deployment

The on orbit deployment phase test results can be broken into three categories: temperature data, pressure data, and accelerometer data. Figure 6 is a collection of graphs that show the time history temperature data for all three boom heatings before inflation. For each, four thermocouples measured temperature; one near the external fold of each stowed tube (thermocouple A) and one as close to the center of each stowed tube as possible (thermocouple B), one on the experiment structure, and one on the experiment computer processor board (Fig. 4). As expected, tube 1, the first tube to run in the experiment, started at the lowest temperature for all readings, followed by tube 2 and tube 3. After the experiment had cold-soaked for 14 days on orbit, the coldest temperature recorded was tube 1 thermocouple A at −35°C. Both the A and B thermocouples mounted to the tubes show similar trends but slightly different histories. This difference is explained by the location of the thermocouples on the interior folds of the stowed tubes. Thermocouple A was more directly exposed to the resistive heaters and thus reads higher over time for all tubes, and also increases at a faster rate for all tubes. Tube 2's folding pattern was different from the other two tubes, which may explain the deviation in measured heating rate from the other two tubes. It is likely that generally the oven heated the tube at the same rate as the other tests, but due to the different folding, the thermocouples were embedded farther from the surface. The start temperatures and rates of heating in the linear regions of the graphs in Fig. 6 are shown in Table 1.

After the tube 1 deployment and postdeployment data collections were complete, tube 2's starting temperature was over 20°C warmer than that of tube 1 due to the radiative and conductive heating effects of the oven operation (Fig. 6, Table 1). The structural heating rates are much higher during the tube 1 deployment than for the tube 2 and 3 deployments. Each experiment for each tube ran to completion separately, meaning that the tube 1 oven was on for a period of time, then off while the deployment, cooling, and vibration test were run, then the tube 2 oven turned on, etc. Each oven was set to the same temperature, so the fact that the experiment was coldest before the tube 1 oven turning on meant that the heating rate is highest (Fig. 6). This discrepancy seems to indicate the resistive heater's radiative and conductive heating effects on structural temperature taper off toward equilibrium as the structure reaches higher temperatures, however, the structural thermocouple placement was also closest to tube 1, which limits the radiative/conductive effects from bay 2 and 3 ovens. In reality, the rate change from tube to tube is most likely caused by both increasing structural temperature and distance from the second and third oven.

It should be noted that tube temperature should reflect the surrounding environment, but this temperature should not have a noticeable effect on the dynamic properties of the tubes below T_g of 125°C. Therefore despite the fact that the tubes were still cooling

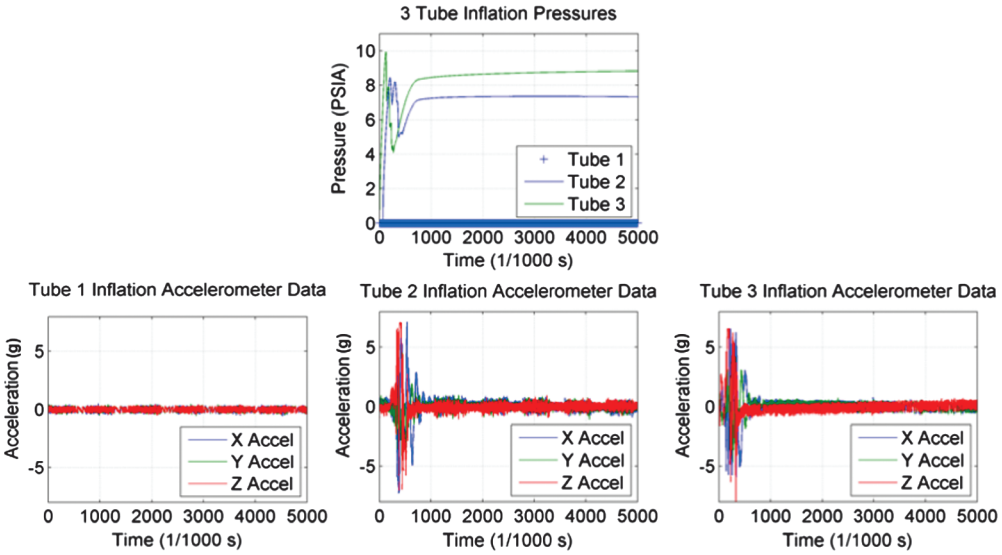

Fig. 7 Deployment pressure and acceleration verse time for all three tubes.

when the vibration tests were run, the fact that all of the tubes were below T_g should negate any thermal effects on the dynamic testing results.

The computer processor board thermocouple readings are also reported in Fig. 6 for completeness and to show the overall temperature increase of the experiment follow the same pattern as the structural thermocouple readings. During tube 1 deployment, the computer thermocouple starts at its lowest reading of −9°C and trends to 0°C over 1000 s. Tube 2 and 3 deployment readings start significantly higher (6.1 and 16.3°C, respectively), but trend at lower rates of 0.007 and 0.004°C/ sec. Again, this is likely attributable to increased temperature reducing radiative heating efficiency and increasing oven distance from the thermocouple. The initial and final temperatures observed by the computer board thermocouple were 15–20°C higher than the structural initial and final temperature; this difference is expected and is a result of the computer heating during operations.

Figure 7 graphically represents the data from the measured pressure inside the tubes and accelerometer readouts during the inflation process following the tube heating. Immediately obvious is the lack of pressure and accelerometer readings from tube 1 indicating that it did not initially inflate. It is belief of the authors that the tube 1 inflation valve suffered from stiction during actuation, and did not open immediately when commanded. This is possibly attributable to the −27°C temperature of the structure at the time inflation was commanded. Postflight inspection, however, shows that tube 1 did in fact inflate, though it is significantly less straight than the other two tubes, which indicates inflation occurred sometime after the tube had partially cooled and became moderately stiff, and after the initial (5 s) pressure and accelerometer data collection ceased. Inflation eventually did occur successfully, however, as pressure was measured in the tube after deployment and during the venting process (see Table 2).

Table 1 Flight temperature data

Thermocouple	Start temp, °C	Rate, °C/s
	Tube 1	
A	−34.0	0.24
B	−17.0	0.19
Structure	−27.0	0.01
Computer	−9.0	0.01
	Tube 2	
A	−11.8	0.17
B	−6.5	0.15
Structure	−7.8	0.004
Computer	6.1	0.007
	Tube 3	
A	−7.5	0.23
B	−0.5	0.18
Structure	−1.0	0.004
Computer	16.3	0.004

Tube 2 and 3 deployments show similar characteristics with an initial and secondary pressure spike attributed to straightening of the folds. The pressure rapidly builds behind the first fold, spiking at 8 and 10 psia for tubes 2 and 3, before the pressure opens the fold enough to allow pressure to begin inflating the tube behind the first fold. At this point, the pressure builds again and pushes through the second fold. There are six folds in the stowed tubes (Fig. 4), four 180° folds and two partial folds. In both tube 2 and 3, there are four spikes in the pressure data, which correlate to pressure building behind each of the four 180° folds.

The triaxial accelerometer data for tubes 2 and 3 reinforces the preceding inflation analysis. Tube 2 does not read any acceleration until the pressure spikes and the inflation gas passes through the first and second folds. At that point acceleration is measured in all three degrees of freedom. Tube 3 generates accelerations above the noise level immediately; the larger pressure spike most likely initiated motion earlier than tube 2, but the tube 3 acceleration spikes are not as distinguishable as the tube 2 acceleration spikes in Fig. 7. As each tube deployed, the accelerometer's coordinate frame rotated with respect to inertial space; thus the x-, y-, and z-axis acceleration data is local to the aluminum end cap.

A slight delay is present in inflation pressure readings for tube 2, which is accompanied by a slightly longer delay in acceleration readings for tube 2. It is believed the tube 2 inflation valve also suffered from a brief bout of cold induced stiction, but rapidly recovered. The additional delay before accelerations were observed for tube 2 and the difference in inflation pressure profile (relative to tube 3) is likely caused by a difference in tube 2's stowed z-fold configuration. Figure 7 also shows that both tubes 2 and 3 inflated in less than 1 s, and tube 1 inflated sometime after 5 s.

Table 2 provides pressure values for the supply tanks and the tubes at discrete points in the experiment timeline. The flight code was programmed to take pressure readings at experiment initialization and at important points in the tube deployment process. Several of the data attributes are immediately recognizable: tube pressure values before commanded inflation are 0 psia and return to 0 psia after commanded venting, the tube and tank pressures are approximately equal after the commanded inflation, tube 1 does register pressure after commanded inflation, tube 2 registers a much lower pressure after commanded inflation than tubes 1 and 3.

As discussed, tube 1 did not inflate while accelerometer and pressure transducer measurements were being recorded, but there are nonzero pressure readings for tube 1 taken 300 s after commanded

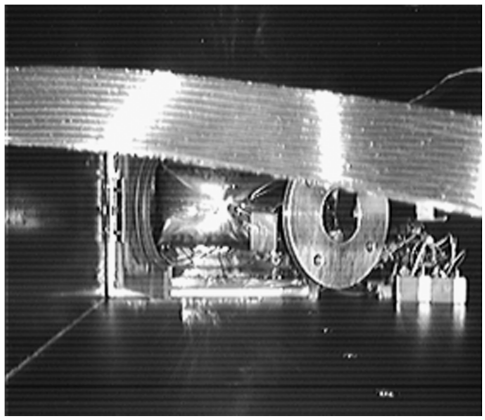

Fig. 8 Tube 1 inflation deployment photo.

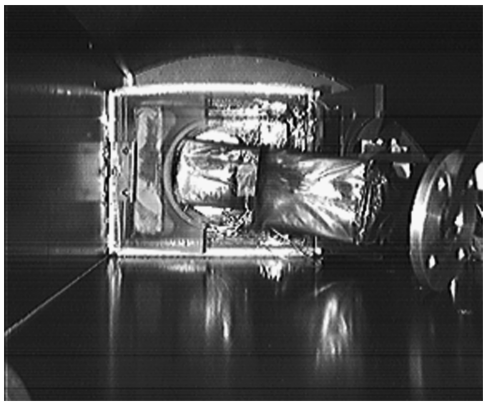

Fig. 9 Tube 2 inflation deployment photo.

inflation. Unfortunately, there were no other pressure readings between commanded inflation +5 and +300 s, so it is not clear as to precisely when the tube inflated. Based on preflight vacuum chamber test results, tube cooling profiles indicate tube 1 probably inflated somewhere within 50 s of the inflation command. Any further delay would have likely resulted in improper deployment as the composite material would have cooled below its glass-transition temperature. Both tubes 1 and 3 read low nonzero pressure after venting was commanded. This indicates venting was mostly (but not entirely) completed in 5 s.

Pressure tank 2 starts with 15% less pressure than the other two tanks, and the equilibrium pressure 300 s after tube 3's commanded inflation is significantly less than tubes 1 and 3 equilibrium pressures (76 and 85%, respectively). It is thought that tube 2 leaked nitrogen after inflation, which may be the explanation for its slightly decreasing pressure at the end of 5 s in Fig. 7, whereas tube 3 slowly increased in pressure. The last tube 2 pressure reading in Fig. 7 is 7.33 psia, much different from the 1.17 psia indicated in Table 1, whereas the last tube 3 pressure reading in Fig. 7 is 8.83 psia, very close to the 8.18 psia cited in Table 2. Tubes 2 and 3 differ by 1.5 psia at the end of Fig. 7. It should be noted that the pressure tanks were filled to approximately 30 psig many months before flight and that the internal volume of each tank and inflation plumbing system was slightly different, so some differences were to be expected. The low pressure in tube 2 indicates that some leakage must have occurred in its tank and inflation plumbing system during cooling, yet the inflated tube appeared normal, indicting robustness in the necessary inflation pressure.

Table 3 CAD, image analysis, and true deployment error dimensions, cm

Analysis type	x	y
	Tube 1	
CAD analysis	x error: −2.90	y error: 0.84
Image analysis	x change: 0.0861	y change: −0.9190
On-orbit deviation	−2.97 cm	1.85 cm
	Tube 2	
CAD analysis	x error: −0.988	y error: −1.244
Image analysis	x change: unknown	y change: unknown
On-orbit deviation	unknown	unknown
	Tube 3	
CAD analysis	x error: 0.150	y error: 0.533
Image analysis	x change: w/in noise	y change: 0.7203
On-orbit deviation	*W/IN NOISE*	0.18 cm

Table 4 Resonant natural frequencies and operating deflection shapes from laser vibrometer

Resonance	Natural frequency, hz	Operating deflection shape comments
	Tube 1	
1	13, 15	First cantilevered bending
2	373	Second cantilevered bending with tip mass
3	787	Second cantilevered bending with tip mass and torsion
6	1792	Fourth cantilevered bending
	Tube 2	
1	28.4, 34.3	First cantilevered bending
2	214	First cantilevered torsion
3	400	Second cantilevered bending with tip mass
4	468,493	Second cantilevered bending with tip mass and torsion
5	765	Second pinned-pinned with breathing
9	1690	Fourth cantilevered bending
	Tube 3	
1	23.9	First cantilevered bending
2	426	Second cantilevered bending with tip mass
3	731	Second cantilevered bending with tip mass and torsion
4	1202	Third cantilevered bending with tip mass and torsion
6	1441	Fourth cantilevered bending with tip mass and torsion

Table 2 Flight tank and tube pressures, psia

Experiment phase	Tank 1 pressure	Tube 1 pressure	Tank 2 pressure	Tube 2 pressure	Tank 3 pressure	Tube 3 pressure
Experiment initialization	14.85	0.00	12.38	0.00	14.48	0.00
Tube 1 initialize	14.83	0.00	12.37	0.00	14.46	0.00
Tube 1 deploy + 300 s	5.26	5.12	12.38	0.00	14.48	0.00
Tube 1 vent + 5 s	5.26	0.10	12.38	0.00	14.48	0.00
Tube 2 initialize	5.26	0.00	12.39	0.00	14.49	0.00
Tube 2 deploy + 300 s	5.28	0.00	1.24	1.17	14.53	0.00
Tube 2 vent + 5 s	5.28	0.00	1.23	0.00	14.53	0.00
Tube 3 initialize	5.28	0.00	1.23	0.00	14.55	0.00
Tube 3 deploy + 300 s	5.30	0.00	1.23	0.00	8.26	8.18
Tube 3 vent + 5 s	5.29	0.00	1.23	0.00	8.26	0.13

Figures 8 and 9 show deployment images of tube 1 and tube 2. These images are taken after the oven door has released and before inflation. Residual strain energy stored during boom stowage has caused the tubes to push slightly out of the ovens. The LEDs provide more than adequate illumination for the pictures, allowing the components to be easily distinguished. Note for tube 1, both oven doors appear to be pushed open, but tube 2 only pushes the right oven door open. These figures give us insight into how the tubes physically deploy in a microgravity environment. The maximum frame rate for the camera was 0.9 s, so only one photo of the deployment process exists for the tubes due to the rapid 1 s inflation as seen in Fig. 7.

All the images taken during flight were further analyzed using image processing. Figure 10 shows an on orbit and postflight image of deployed tube 3 and a composite image resulting from subtracting intensities of the two pixel by pixel. By subtracting intensities, the physical change in the tube endcap position from the on orbit image to the postflight image can be determined. This relative change in position can then be combined with precision ground-based knowledge to determine on orbit deployment accuracy, discussed later. Unfortunately, the camera for tube 2 was inoperable during postflight testing AFIT, so no postflight images are available for tube 2.

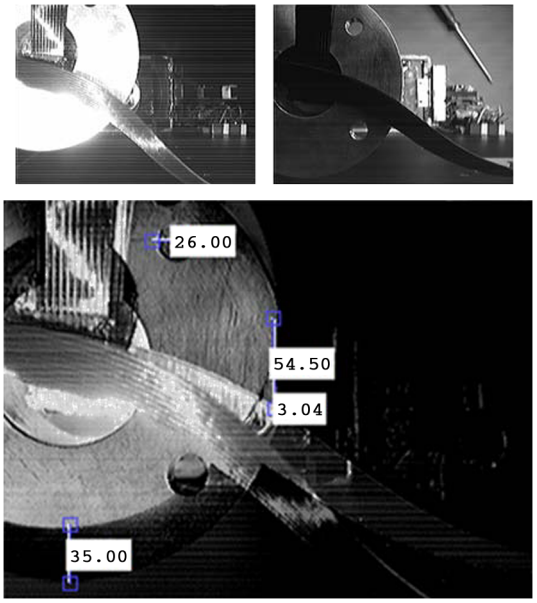

Fig. 10 On-orbit, postflight, and composite image.

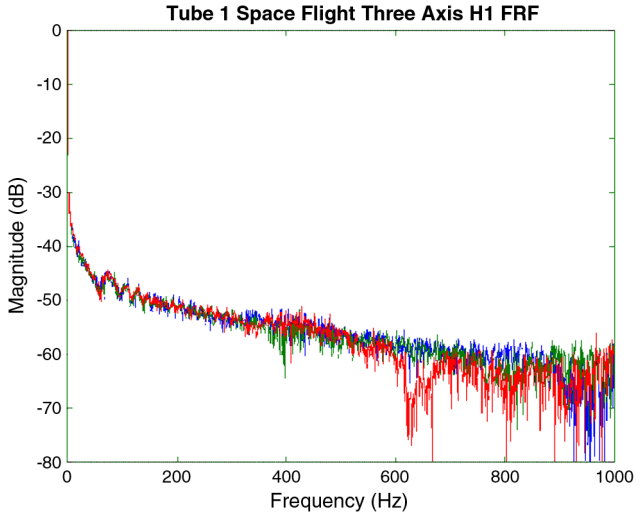

Fig. 11 On-orbit vibration response test *x*, *y*, and *z*-axis H1 0–1000 Hz FRF.

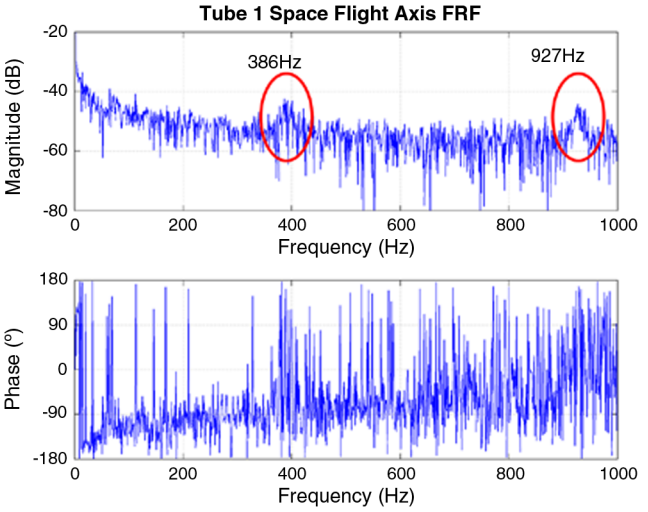

Fig. 12 Tube 1 *x*-axis 0–1000 Hz H1 FRF.

The preceding data show the effectiveness of the heating and inflation system used on RIGEX. All three tubes successfully deployed despite lower than anticipated starting temperatures. The data show that the resistive heaters successfully warmed the tubes, that deployment occurred in under 1 s, and the tubes were able to hold pressure long enough to cool and rigidize. These results constitute the successful completion of the primary experimental objectives.

B. Postdeployment

The postdeployment phase ground analysis focused on comparing the on orbit vibration response of the deployed tubes to what was obtained on the ground. The auto and cross spectral power densities of the input (input chirp signal) and output (accelerometer readings) for each of the 25 test iterations were averaged to help reduce the noise in the sampled signals. The input chirp signal is shown in Eq. (1), and provided input voltage $y(t)$ as a function of time t. This signal provided excitation of 0–2000 Hz for each of the 25 vibration test iterations:

$$y(t) = \cos(2\pi(5 + (1000 - 5)t)t) \tag{1}$$

The averaging of the data was necessary to improve the sampled results due to the low signal to noise ratio. The averaged FRFs, however, had no resonant natural frequency peaks, which was unexpected (Fig. 11). Preflight test results predicted resonances around 60, 250, and 660 Hz [23]. Design limitations prevented recording the actual input signal seen by the piezoelectric patches,

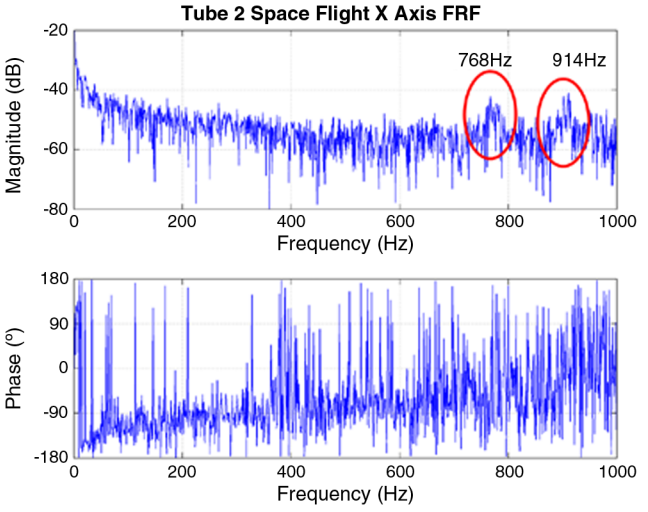

Fig. 13 Tube 2 *x*-axis 0–1000 Hz H1 FRF.

meaning that to maintain simplicity of the design no digital to analogue converter was included in the system.

Each iteration of the vibration response test was analyzed separately, and all contained peaks, although the peaks did not occur at consistent frequencies across the tubes or even within the 25 sample sets from the same tube. Given the frequency variability, the 25 individual FRFs are presented on the same plot. Figures 12–14 are the final test iteration *x*-axis FRF for tubes 1–3, and Figs. 15–17 are the 25 individual *x*-axis FRFs for tubes 1–3, plotted by iteration rather than amplitude. Figures 15–17 are a top view of the 25 FRFs, with the shading representing amplitude to clearly highlight the resonance peaks (dark). As the figures indicate, the resonance frequencies shifted between test iterations during the space flight vibration response test. The initial analysis efforts' averaging process in Fig. 11 had therefore washed out the resonant peaks in the averaged FRF because the peaks appear at different frequencies at each iteration. This variation is believed to be a result of a data sample storage timing anomaly in the RIGEX computer which rendered the frequency content of the sampled data inaccurate rather than nonlinear time dependant dynamic response.

Another possible contributing complication is that the tubes were covered in Kapton tape which could have caused them to cool at a slower rate than in ground thermal vacuum testing. However, even if the tube was still very warm, preflight tests indicated increased temperature has no dramatic effect on the structural behavior of the tubes up to 100°C [24].

An additional complication resulted from the lower than expected signal level during the vibration test. The MFCs providing the excitation signal are epoxied to the tube near the base cap, and remain inside of the oven box after the tube has deployed. It is possible the oven insulation prevented the lower portion of the tube from cooling as rapidly as preflight ground testing suggested, which may have left the base slightly flexible during vibration testing, producing lower than expected moments from the MFCs. Again, the temperature of the base of the tube was not recorded at the start of the vibration response testing, but the postdeployment image of flight tube 3 indicates the oven doors had closed after deployment (flight tubes 1 and 2 oven doors remained open). The closed oven doors could trap more heat and result in lower than expected excitation levels.

Unfortunately since RIGEX was a flight prototype, a fully-independent end-to-end system test replicating the entire experiment on the ground was not performed.

C. Postflight

Concerned about any potential hazards that could occur during shipping from Kennedy Space Center to AFIT, the recorded experiment data was copied from the flight computer and several

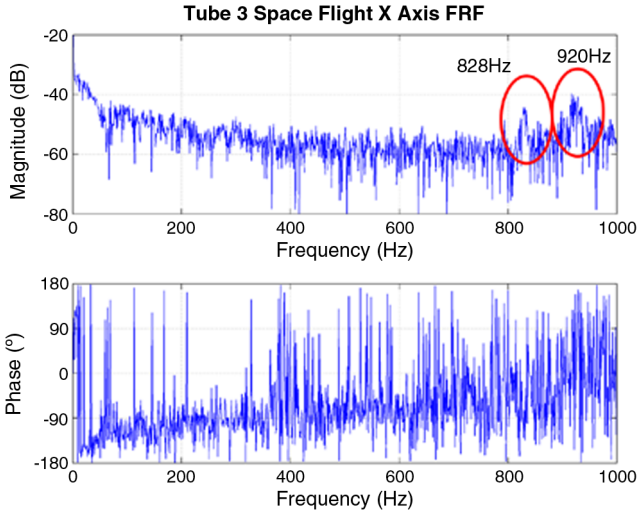

Fig. 14 Tube 3 *x*-axis 0–1000 Hz H1 FRF.

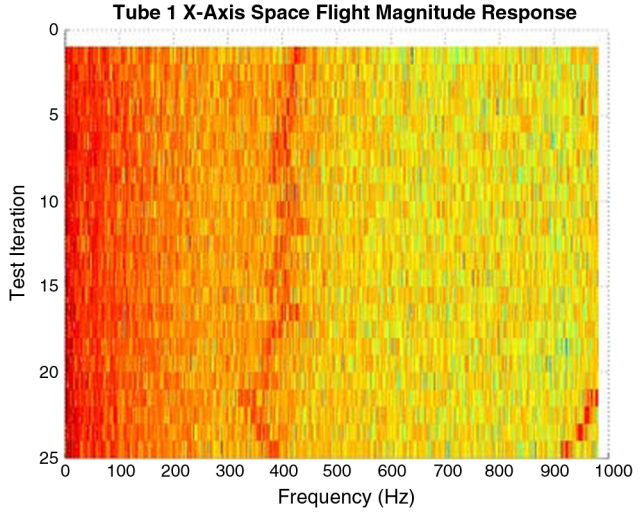

Fig. 15 Tube 1 *x*-axis 0–1000 Hz H1 FRF demonstrating resonance peak drift.

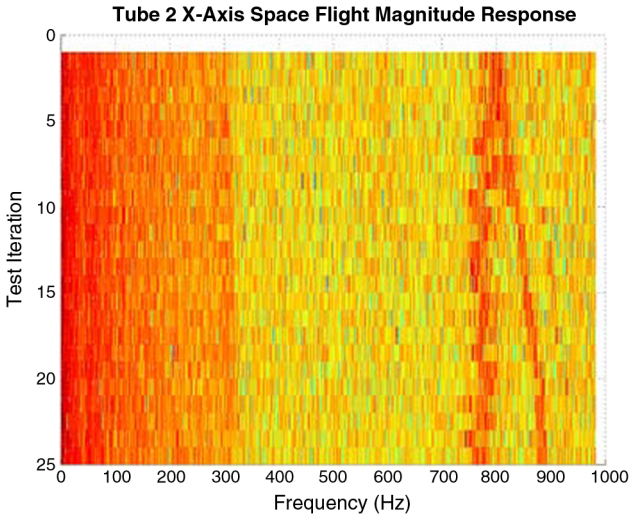

Fig. 16 Tube 2 *x*-axis 0–1000 Hz H1 FRF demonstrating resonance peak drift.

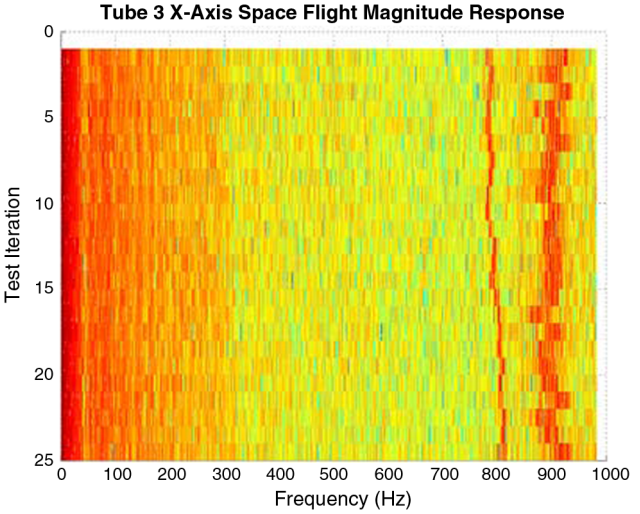

Fig. 17 Tube 3 *x*-axis 0–1000 Hz H1 FRF demonstrating resonance peak drift.

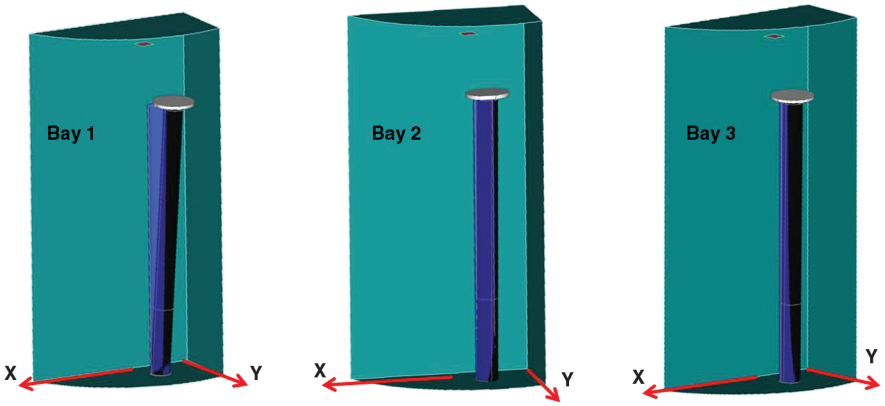

Fig. 18 Measured deployment of each tube (black) overlaid on a true deployment (blue).

pictures were taken of the successfully deployed tubes. Upon return to AFIT, the first task was to perform a three-dimensional scan of the experiment accurate to 1 mm.

Measurements were taken of the camera, bay walls, tube top end cap, and the tube itself for all three bays without disassembling the experiment. The carbon fiber tube could only be measured from the tube tip through the top of the oven, as the oven prevented the probe from going any lower. While measuring along the length of the tube, care was taken to not move the tube with the hard probe: doing so would lower the accuracy of the hard probe measurements. Planes were fit to the three-dimensional bay wall and camera point clouds, cylinders were fit to the tubes and top end caps, with another plane fit to the top of the end cap.

The three geometry files (one per bay) were imported into a CAD package for further processing. A linear extrapolation of the cylinder fit to each tube was extended to the floor of the bay to complete the model of the deployed tubes. Using the as-built drawings [25,26], an ideal deployed tube was then modeled to compare to the tubes deployed in space, centered on the exact location of the tube mount for comparison purposes. First, the horizontal planar x- and y-axis differences between the ideal and flight tubes were measured; this, in essence, is the deviation from true, or perfectly straight. Only the horizontal plane deviation calculations were conducted. The vertical differences were not measured due to the influence of potential manufacturing defects and the creases remaining from the major folds would increase the order of uncertainty beyond the error measurements themselves. The intersection of the ideal and flight tubes with the floor of the bay lines up very well for all three bays; the deviation at the bottom between true and deployed is the genesis of the order of error in the horizontal plane deviation measurements.

Figure 18 shows the finished geometry models. The perfectly deployed tubes are represented with light cylinders, and the actual deployed tubes are shown with representative dark tubes a silver top flange (similar to the carbon fiber and aluminum end cap). Table 3 lists the measured CAD deviations from straight and the results of the image change analysis discussed previously. The CAD analysis measures the deviation from nominal (perfectly straight) for the postflight tubes. The image change analysis measures the change from in space deployed position to postflight measured at AFIT

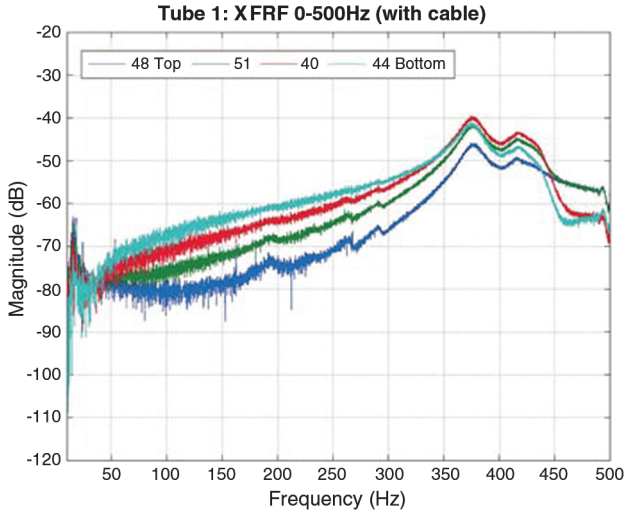

Fig. 19 Tube 1 four 0–500 Hz x-Axis FRFs.

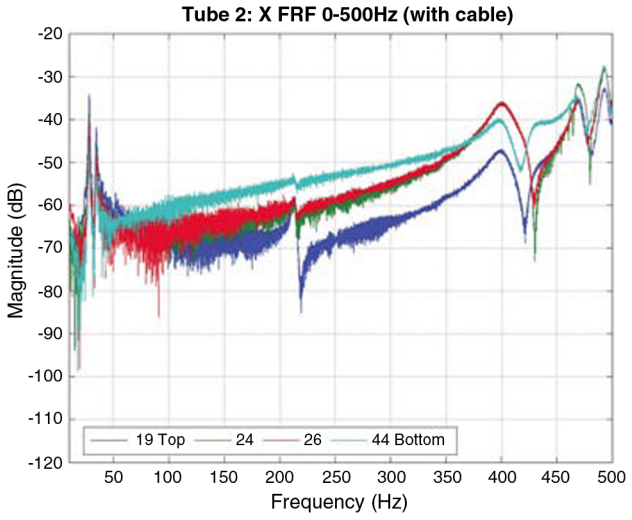

Fig. 20 Tube 2 four 0–500 Hz x-Axis FRFs.

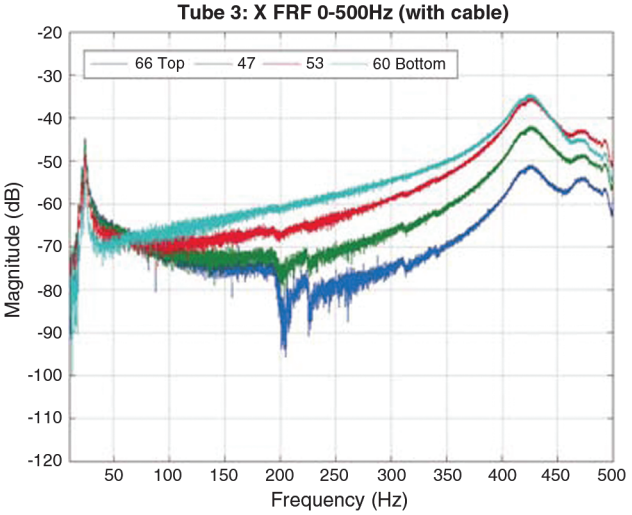

Fig. 21 Tube 3 four 0–500 Hz x-Axis FRFs.

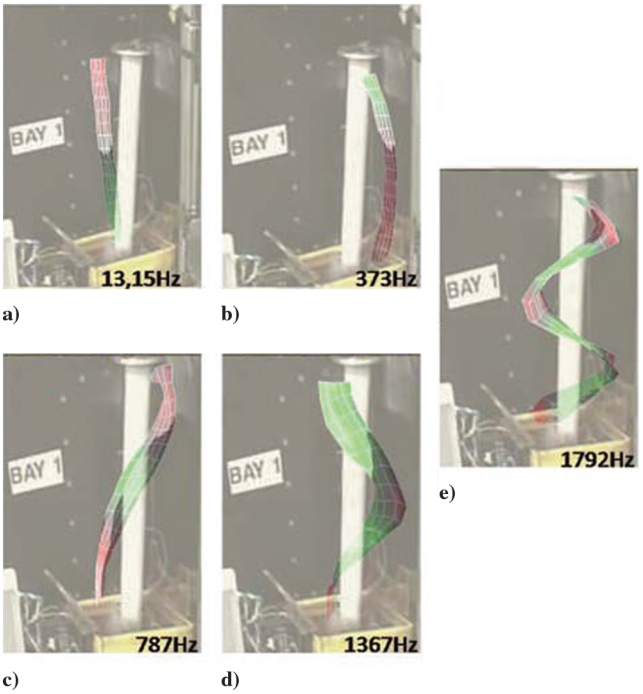

Fig. 22 Tube 1 operating deflection shapes and natural frequencies.

deployed position caused by landing, shuttle removal, shipping, etc. Combining these two measurements yields the deployment deviation from nominal (perfectly straight) on orbit, and is reported in Table 3.

As expected, tube 1 shows the largest error, assumed to be a result of the delayed inflation. The on orbit deviation of tube 2 is indeterminable (because of a lack of a postflight image for change detection), but the on orbit deviation of tube 3 was virtually zero, meaning it deployed almost perfectly true on orbit. Even without the image analysis, tube 2 deviation was quite small. This is excellent evidence that precision on orbit deployment is feasible with these subglass-transition inflatable/rigidizable tubes. The accuracy of these measurements is limited by the resolution of the cameras. In this case, one pixel covers approximately 5 mm, depending on how far the object is from the camera.

The scanning laser vibrometer test results round out the postflight analysis. The 0–500 Hz measured FRFs are shown in Figs. 19–21 for tubes 1, 2, and 3, and Fig. 22 presents operating deflection shapes for tube 1. Figures 19–21 each contain four respective FRFs which correspond to different scan point on each tube. The presented scan points are arranged vertically on the respective tube, such that the response of the scan point near the bottom of the tube is presented with the response of the scan point near the top of the tube, and then two other scan points along the tube. In the operating deflection shape montages, all of the scan points are presented and overlaid on the target tube to present a magnified picture of the deflection shape of the scanned area in Fig. 22.

The first resonant natural frequency observed in the postflight testing that correlates with the on orbit data is the second cantilevered bending mode (373 Hz in Fig. 19, shape B in Fig. 21), which matches fairly well with the observed 386 Hz mode in Fig. 12. Also, note tube 2 has a resonance at 214 Hz–: this is a cantilevered torsion mode, which was not readily identified in tubes 1 and 3. Tube 2 also has a strong split in the first cantilevered bending mode. Curiously, tube 2 has a stiffer first bending mode (for the split peaks) than tube 3, but tube 3 has a significantly stiffer second cantilevered bending mode (with tip mass). The resonant frequencies and operating deflection shape summaries are provided in Table 4, corresponding to standard cantilevered hollow beam mode shapes. The results show substantial variability in structural natural frequencies from one tube to the next (though it is difficult to compare tube 1 to the other two due to the delayed inflation), demonstrating the difficulty of effectively measuring these types of structures and the need for further testing and predictive modeling.

V. Conclusions

RIGEX completed its primary experimental objectives by successfully inflating and rigidizing carbon fiber composite booms in space. Temperature, pressure, image, and accelerometer data were all successfully collected on orbit and retrieved for processing. The data shows the ovens performed flawlessly and appear as though they could be reused, important information for consideration in deploying multiple booms on orbit. As designed, the ovens increased the experiment structure temperature significantly during tube heating and the structure appeared to be headed toward thermal equilibrium in space. The single latch and shape memory alloy pin pullers were a simple but effective method of opening the ovens. Thermal couples mounted within the tube folds with Kapton tape effectively measured the T_g of the tubes.

Tube 3 inflated immediately after the inflation solenoid was commanded open, but tube 2 had a 0.068 s delay, and tube 1 did not inflate while the inflation pressure was being monitored for 5 s following the inflation command, but it did inflate within 50 s of the command. Also, recorded on orbit inflation pressure spikes were correlated to the opening of pressure seals created by folds in the stowed tubes. The commercial off the shelf low pressure valve and sensing were proven adequate for this experiment.

The imaging system worked as advertised on orbit, and through a combination of image change detection analysis and high resolution contact measurement, the exact on orbit deployment error of tube 1 was determined to be −2.87 and 1.85 cm in the respective x and y-axis. Tube 3 achieving an almost perfectly straight deployment on orbit (within measurement noise and 0.18 cm for x and y-axis, respectively)–critical information for precision inflatable deployment necessary for joining large structures on orbit. Variation was observed between the three tubes, the deployments of which were designed to be nearly identical.

The flight booms exhibited lower natural frequencies on orbit than were measured in the preflight tests on the ground. During the space flight vibration testing, the resonant frequencies were measured, though at an unexpectedly-low signal to noise level. From the available data, the flight vibration response test results consist of a few peaks which mostly correlated to postflight vibration response tests. Overall, the first and second bending modes of all three flight tubes and the first torsional mode of flight tube 2 were comparable (but typically at lower frequencies) to the preflight testing modes. The MFC patches used for excitation appeared to perform flawlessly as expected in space, and were used as-is for all subsequent ground tests postflight.

Overall, the RIGEX experiment achieved all of its objectives and generated new avenues for scientific inquiry. It was a successful proof of concept demonstration of rigidizable inflatable booms, and results in a TRL increase of rigidizable/inflatable technology for space applications.

Acknowledgments

The authors would especially like to thank Brett Cooper, Jeremy Owens, John DiSebastian, Jeremy Goodwin, Anna Gunn-Golkin, Sarah Helms, Raymond Holstein, Steven Lindemuth, Zachary Miller, Chad Moeller, David Moody, Brady O'Neal, Thomas Philley, and Thomas Single, the students who were each a part of the Rigidizable Inflatable Get-Away-Special Experiment (RIGEX) program during different phases of the experiment development and are responsible its overall success. The authors would like to thank Jay Anderson, Sean Miller, and Wilbur Lacy of the Air Force Institute of Technology for all of their dedication and time. The authors would also like to thank Greg Agnes and Keats Wilkie of NASA for their support. L'Garde, Inc., supplied the rigidizable inflatable tubes. RIGEX was integrated and flown under the direction of the Department of Defense's Space Test Program.

References

[1] Jenkins, C. M. H., ed., *Gossamer Spacecraft: Membrane and Inflatable Structures Technology for Space Applications*, Progress in Astronautics

and Aeronautics, Vol. 191, AIAA, Reston, VA, 2001.
[2] Wertz, J. R., and Larson, W. J., *Space Mission Analysis and Design*, 3rd ed., Microcosm, 1999.
[3] *Bigelow Aerospace Inflatable Habitats*, www.bigelowaerospace.com [retrieved Jan. 2009].
[4] Pappa, R. S., Lassiter, J. O., and Ross, B. P., "Structural Dynamics Experimental Activities in Ultralightweight and Inflatable Space Structures," *Journal of Spacecraft and Rockets*, Vol. 40, No. 1, Jan.–Feb. 2003, pp. 15–23.
doi:10.2514/2.3934
[5] Derbès, B., "Case Studies in Inflatable Rigidizable Structural Concepts for Space Power," AIAA Paper 1999-1089, 37th AIAA Aerospace Sciences Meeting, Reno, NV, Jan. 1999.
[6] Watson, J. J., "Static-Test Results for the Characterization of Inflatable Rigidizable Columns," AIAA Paper 2001-1269, 42nd AIAA/ASME/ASCE/AHS/ASC Structures, Structural Dynamics and Materials Conference, Seattle, WA, April 2001.
[7] Wilkie, W. K., Bryant, R. G., High, J. W., Fox, R. L., Hellbaum, R. F., Jalink, A., Jr., Little, B. D., and Mirick, P. H., "Low-Cost Piezocomposite Actuator for Structural Control Applications," *Proceedings of SPIE: The International Society for Optical Engineering*, Vol. 3991, March 2000.
doi:10.1117/12.388175.
[8] Rivas McGowan, A. M., Wilkie, W. K., Moses, R. W., Lake, R. C., Florance, J. P., Wieseman, C. D., Reaves, M. C., Taleghani, B. K., Mirick, P. H., and Wilbur, M. L., "Aeroservoelastic and Structural Dynamics Research on Smart Structures Conducted at NASA Langley Research Center," *Proceedings of SPIE: The International Society for Optical Engineering*, Vol. 3326, March 1998, pp. 188–201.
[9] Engberg, R. C., and Lassiter, J. O., "Dynamic Testing of Inflatable Spacecraft Structures," *Sound and Vibration*, June 1999, pp. 16–20.
[10] Engberg, R. C., Lassiter, J. O., and McGee, J. K., "Modal Survey Test of the SOTV 2×3 Meter Off-Axis Inflatable Concentrator," AIAA Paper 2000-1639, 41st AIAA/ASME/ASCE/AHS/ASC Structures, Structural Dynamics, and Materials Conference, Atlanta, GA, April 2000.
[11] Slade, K. N., Tinker, M. L., Lassiter, J. O., and Engberg, R., "Comparison of Dynamic Characteristics for an Inflatable Solar Concentrator in Atmospheric and Thermal Vacuum Conditions," AIAA Paper 2000-1641, 41st AIAA/ASME/ASCE/AHS/ASC Structures, Structural Dynamics, and Materials Conference, Atlanta, GA, April 2000.
[12] Slade, K., Virgin, L., and Tinker, M., "Mode Splitting in an Inflated Polyimide Cylinder with Circumferential Asymmetry," AIAA Paper 2001-1411, 42nd AIAA/ASME/ASCE/AHS/ASC Structures, Structural Dynamics, and Materials Conference, Seattle WA, April 2001.
[13] Griffith, D. T., and Main, J. A., "Modal Testing of an Inflated Thin Film Polyimide Torus Structure," *Proceedings of IMAC 18*, Feb. 2000, pp. 1035–1041.
[14] Griffith, D. T., and Main, J. A., "Experimental Modal Analysis and Damping Estimation of an Inflated Thin-Film Torus," *Journal of Guidance, Control, and Dynamics*, Vol. 25, No. 4, 2002, pp. 609–617.
doi:10.2514/2.4934
[15] Ruggiero, E. J., "Active Dynamic Analysis and Vibration Control of Gossamer Structures Using Smart Materials," Masters Thesis, Virginia Polytechnic Institute and State University, Blacksburg, VA, May 2002.
[16] Park, G., Ruggiero, E., and Inman, D. J., "Dynamic Testing of Inflatable Structures Using Smart Materials," *Smart Materials and Structures*, Vol. 11, No. 1, 2002, pp. 147–155.
doi:10.1088/0964-1726/11/1/317
[17] Ruggiero, E. J., Bonnema, G. T., and Inman, D. J., "Application of SISO and MIMO Modal Analysis Techniques on a Membrane Mirror Satellite," *Proceedings of 2003 ASME International Mechanical Engineering Congress and Exposition*, Aerospace Division, Washington, D.C., Nov. 2003, pp. 63–69.
[18] Sodano, H. A., Park, G., and Inman, D. J., "An Investigation into the Performance of Macro-Fiber Composites for Sensing and Structural Vibration Applications," *Mechanical Systems and Signal Processing*, Vol. 18, No. 3, 2004, pp. 683–697.
doi:10.1016/S0888-3270(03)00081-5
[19] Ruggiero, E. J., Park, G., and Inman, D. J., "Multi-Input Multi-Output Vibration Testing of an Inflatable Torus," *Mechanical Systems and Signal Processing*, Vol. 18, No. 5, Sept. 2004, pp. 1187–1201.
doi:10.1016/j.ymssp.2004.01.003
[20] Song, H., Smith, S. W., and Main, J. A., "Dynamic Testing of an Inflatable, Self-Supporting, Unpressurized Thin Film Torus," *Journal of Guidance, Control, and Dynamics*, Vol. 29, No. 4, July–Aug. 2006, pp. 839–845.
doi:10.2514/1.16509
[21] Cobb, R., Black, J., and Swenson, E. D., "Design and Flight Qualification of the Rigidizable Inflatable Get-Away-Special Experiment," *Journal of Spacecraft and Rockets*, Vol. 47, No. 4, July–Aug. 2010, pp. 659–669.
doi:10.2514/1.48636also AIAA Paper 2009-2155.
[22] Department of Defense Shuttle/International Space Station Payload Support Contract, Muniz Engineering, "Container for All Payload Ejections (CAPE) Hardware Users Guide (CHUG)," NASA Johnson Space Center [retrieved March 2003].
[23] Owens, J. J., "Final Assembly, Testing and Processing of the Rigidizable Inflatable Get-Away-Special Experiment (RIGEX) for Spaceflight Qualification," Master's Thesis, Air Force Institute of Technology, Wright–Patterson AFB, OH, Sept. 2007, http://www.dtic.mil/cgi-bin/GetTRDoc?AD=ADA522020&Location=U2&doc=GetTRDoc.pdf [retrieved April 2010].
[24] Moeller, C. R., "Design and Ground-Testing of an Inflatable-Rigidizable Structure Experiment in Preparation for Spaceflight," Master's Thesis, Air Force Institute of Technology, Wright–Patterson AFB, OH, June 2005, http://www.dtic.mil/cgi-bin/GetTRDoc?AD=ADA437936&Location=U2&doc=GetTRDoc.pdf [retrieved April 2010].
[25] Single, T. G., "Experimental Vibration Analysis of Inflatable Beams for an AFIT Space Shuttle Experiment," Master's Thesis, Air Force Institute of Technology, Wright–Patterson AFB, OH, March 2002, http://www.dtic.mil/cgi-bin/GetTRDoc?AD=ADA401458&Location=U2&doc=GetTRDoc.pdf [retrieved April 2010].
[26] Philley, T. L., "Development, Fabrication, and Ground Test of an Inflatable Structure Spaceflight Experiment," Master's Thesis, Air Force Institute of Technology, Wright–Patterson AFB, OH, March 2003, http://www.dtic.mil/cgi-bin/GetTRDoc?AD=ADA413193&Location=U2&doc=GetTRDoc.pdf [retrieved April 2010].

J. Martin
Associate Editor